

Nuclear Excitation by Near-Resonant Electron Transition in $^{229}\text{Th}^{39+}$ Ions

Karol Koziol* and Jacek Rzadkiewicz†

Narodowe Centrum Badań Jądrowych (NCBJ), Andrzeja Soltana 7, 05-400 Otwock-Świerk, Poland

Theoretical considerations are made for the nuclear excitation from the ground state to the 8 eV ^{229m}Th isomer via near-resonant electron transitions in Sb-like ($q = 39+$) thorium ions. The energy of the first excited atomic state ($J = 7/2$) in the $^{229}\text{Th}^{39+}$ ion is estimated to be 8.308 ± 0.011 eV, which is very close to the new reference value for the ^{229m}Th nuclear isomer energy, 8.338 ± 0.024 eV [Kraemer et al., *Nature* 617, 706 (2023)]. It was found that within the uncertainty range of both atomic and nuclear excitation energies, the rate of nuclear excitation by electron transition can vary by more than 20 orders of magnitude. Our results indicate that the upper theoretical limit for the ^{229m}Th isomer excitation rate reaches an enormous value of $1.05 \times 10^{16} \text{ s}^{-1}$ at resonance ($\Delta = 0$ meV). Additionally, it was shown that using an electron beam ion trap (EBIT), the production of the ^{229}Th isomer can reach rates ranging from tenths to approximately $6 \times 10^{19} \text{ s}^{-1}$. Thus, EBIT experimental studies could serve as an extremely sensitive tool for the independent verification of the excitation energy of the isomeric state in the ^{229}Th nucleus.

There is strong interdisciplinary interest in the ^{229}Th isotope due to its potential applications, such as serving as a nuclear clock frequency standard [1–3] and allowing for precise determination of the temporal variation of fundamental constants [4–6]. This interest is particularly focused on its metastable first excited state, ^{229m}Th ($3/2^+$, $T_{1/2} = 1740 \pm 50$ s [7]), which is approximately 8 eV above the nuclear ground state – several orders of magnitude lower than typical nuclear excitation energies. Recent experimental values for the ^{229m}Th isomer excitation energy (since 2019) range from 8.1 eV to 8.3 eV [8–10]. The most recent experiment, performed using VUV spectroscopy of ^{229m}Th incorporated into CaF_2 and MgF_2 crystals at the ISOLDE facility at CERN, resulted in an excitation energy of 8.338 ± 0.024 eV [11].

Progress in experimental techniques, particularly in manipulating high-charged ions (HCIs), has opened new avenues for driving the isomeric transition. Several methods have been proposed to excite the ^{229}Th nucleus from its ground state to various excited isomeric states [3]. A controlled excitation of the ^{229}Th ground state to the second excited state ($5/2^+$, $E = 29.19$ keV, $T_{1/2} \sim 100$ ps) has recently been achieved through x-ray pumping with synchrotron radiation [12]. Additionally, the production of ^{229m}Th by exciting the ^{229}Th ground state to the second excited state at 29.19 keV via nuclear excitation by electron capture (NEEC) has been proposed [13]. Other proposed methods for exciting the ^{229}Th isomer include nuclear excitation via electronic resonance [14–17] and via defect states in doped crystals [18]. The potential for nuclear excitation through electron transfer (NEET), two-photon electron transitions (NETP), or electronic bridge excitation (EBE) of the ^{229}Th isomer has also been theoretically investigated for Th^+ [15, 19, 20], Th^{2+} [16, 20, 21], Th^{3+} [14, 20], and Th^{35+} ions [17, 22].

In this work, we investigate nuclear excitation by near-resonant electron transition in Sb-like ($^{229}\text{Th}^{39+}$) thorium ions with the $[\text{Kr}]4\text{d}^{10}4\text{f}^5$ electronic configuration. In the NEET process, the energy of electron transition in

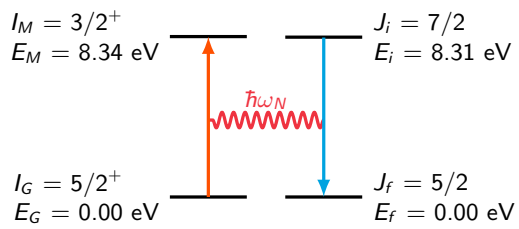


FIG. 1. NEET mechanism in $^{229}\text{Th}^{39+}$ ions.

an atom is transferred to the excitation of the nucleus. This transfer can be particularly effective if the nuclear excitation energy matches the electron transition energy. In the $^{229}\text{Th}^{39+}$, the ground state transition from the first atomic excited state seems to meet this condition. Therefore we attempted to precisely determine the energy of this transition and its intensity (natural width of the state). Since experimental data are not available for the low-energy atomic states of Th^{39+} ions, in our analyzes we employed the Multi-Configuration Dirac–Hartree–Fock (MCDHF) method with Configuration Interaction (CI). By using the atomic transition energy and the widths of the appropriate atomic states together with the most accurate estimates of the energy and width of the ^{229m}Th isomer [11], we estimate the NEET rates for Th^{39+} ions. In addition, the low-energy atomic structure of Th^{39+} ions was analyzed. Using this structure, an experimental scenario for an electron beam ion trap (EBIT), which would allow for rigorous verification of the ^{229m}Th isomer excitation energy is considered. The scheme of the NEET mechanism for the $^{229}\text{Th}^{39+}$ ion is shown in Fig. 1.

The calculations of the energy levels for the Th^{39+} thorium ion were performed using the GRASP2018 code [23], which implements the MCDHF-CI method. The methodology employed in this study is similar to previous work (see, e.g., [24–26]) and is based on a fully relativistic Dirac Hamiltonian and a multi-configurational expansion of the Atomic State Function. In the present calculations, we

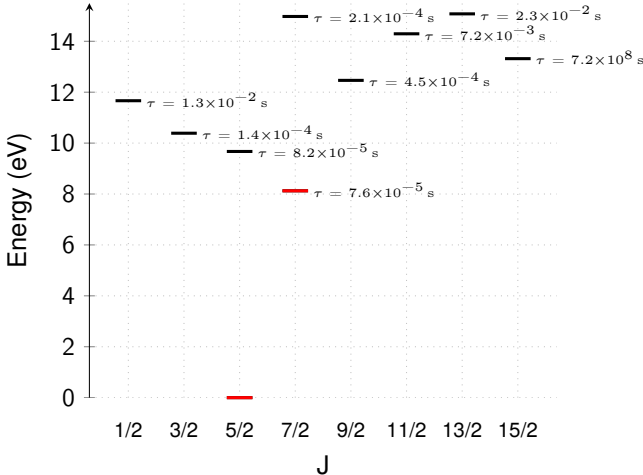


FIG. 2. Energy level diagram for the ten lowest-lying states of the $[{\rm Kr}]4{\rm d}^{10}4{\rm f}^5$ configuration of Th^{39+} . The radiative lifetime values are indicated next to the level markers.

used active spaces (AS) of virtual orbitals with principal quantum numbers n up to 7 and angular momentum quantum numbers l up to 5. The multireference (MR) set includes all Configuration State Functions (CSFs) corresponding to the $[{\rm Kr}]4{\rm d}^{10}4{\rm f}^5$ electronic configuration. We explored the extension of the active space by increasing both the number of occupied orbitals, from which single (S) and double (D) substitutions are made, and the number of virtual orbitals to which these substitutions are applied. In this work, we utilized active spaces denoted as AS x (4f), AS x (4df), AS x (4pdf), and AS x (4spdf). The AS x (4f) active space includes SD substitutions from the 4f subshell, while AS x (4df) includes SD substitutions from both the 4d and 4f subshells, and so forth. The $n = 1, 2, 3$ shells are treated as the inactive core. The notation x refers to the highest principal quantum number of the virtual orbitals; for example, in the AS1 active space, the highest n of the orbitals is 4, while in AS2 it is 5, and so on. The Extended Optimal Level (EOL) scheme [27] was employed to calculate the radial wavefunctions of the considered levels. In this scheme, the radial wavefunctions are optimized for all states related to the given electron configuration, averaged with the weights of $(2J + 1)$. We calculated the Breit term in the low-frequency limit, as a frequency-dependent term is not appropriate for virtual orbitals [28].

The total number of calculated levels for the given J^p symmetry of the $[{\rm Kr}]4{\rm d}^{10}4{\rm f}^5$ configuration is as follows: 10 levels for $1/2^-$ symmetry, 21 for $3/2^-$, 28 for $5/2^-$, 30 for $7/2^-$, 29 for $9/2^-$, 26 for $11/2^-$, 20 for $13/2^-$, 16 for $15/2^-$, 9 for $17/2^-$, 5 for $19/2^-$, 3 for $21/2^-$, and 1 for $23/2^-$. Due to the rapid increase in the size of the expansions with the growth of the MR set, the AS2(4df) level of calculations was employed in this case. Calculated electronic energy levels for the ten lowest-

TABLE I. Energy of the $J = 7/2$ level relative to the $J = 5/2$ ground state of Th^{39+} for various active spaces.

Active space	Excitations				E (eV)	
	from		to			
	SD	S only	SD	S only		
MR = AS1(4f)	4f		4f		7.993	
AS2(4f)	4f		$\leq 5\text{spdfg}$		8.140	
AS3(4f)	4f		$\leq 6\text{spdfgh}$		8.150	
AS4(4f)	4f		$\leq 7\text{spdfgh}$		8.151	
AS1(4df)	4df		$\leq 4\text{df}$		8.177	
AS2(4df)	4df		$\leq 5\text{spdfg}$		8.245	
AS3(4df)	4df		$\leq 6\text{spdfgh}$		8.203	
AS4(4df)	4df		$\leq 7\text{spdfgh}$		8.199	
AS1(4pdf)	4pdf		$\leq 4\text{pdf}$		8.243	
AS2(4pdf)	4pdf		$\leq 5\text{spdfg}$		8.386	
AS3(4pdf)	4pdf		$\leq 6\text{spdfgh}$		8.290	
AS4(4pdf)	4pdf		$\leq 6\text{spdfgh}$	7spdfg	8.288	
AS1(4spdf)	4spdf		$\leq 4\text{spdf}$		8.261	
AS2(4spdf)	4spdf		$\leq 5\text{spdfg}$		8.408	
AS1*(4spdf)	4pdf	4s	$\leq 4\text{spdf}$		8.243	
AS2*(4spdf)	4pdf	4s	$\leq 5\text{spdf}$		8.419	
AS3*(4spdf)	4pdf	4s	$\leq 6\text{spdfgh}$		8.310	
AS4*(4spdf)	4pdf	4s	$\leq 6\text{spdfgh}$	7spdfg	8.308	
reference value					8.308(11)	

lying states of the $[{\rm Kr}]4{\rm d}^{10}4{\rm f}^5$ configuration of the Th^{39+} ion, categorized by their angular momentum quantum number J groups, are shown in Fig. 2. Energies and LS -compositions of all $[{\rm Kr}]4{\rm d}^{10}4{\rm f}^5$ levels are listed in the table in the Supplementary Material, and a graphical representation of the level arrangement is also presented in the Supplementary Material. As illustrated in Fig. 2, the energy difference between the ground state of $J = 5/2$ and the first excited state of $J = 7/2$ is approximately 8 eV, which is very close to the excitation energy of the isomeric state in the ^{229}Th nucleus. Notably, the $J = 15/2$ atomic state at 13 eV has an extraordinarily long radiative lifetime, on the order of 10^8 s. The dominant radiative de-excitation channel for the $J = 15/2$ state is the weak M3 transition to the $J = 9/2$ state, with a rate of $3.9 \times 10^{-20} \text{ s}^{-1}$. The sum of hyperfine-induced transition rates from the $J = 15/2$ level to the possible lower levels (calculated using the MITHIT code [29], based on GRASP2018 data) is $1.4 \times 10^{-9} \text{ s}^{-1}$. The population of this $J = 15/2$ state, along with all cascade transitions leading to it, would reduce the relative population of the first excited state ($J = 7/2$), which is necessary to initiate the NEET process in the Th^{39+} ion.

As mentioned above, the recent analysis estimates the excitation energy for ^{229}Th to be 8.338 ± 0.024 eV [11]. Therefore, we focused on the atomic transitions between the first excited state ($J = 7/2$) and the ground state ($J = 5/2$). Energies of the $J = 7/2$ level related to the $J = 5/2$ ground state of the Th^{39+} ion for various active spaces are presented in Table I and Fig. 3. In the calcula-

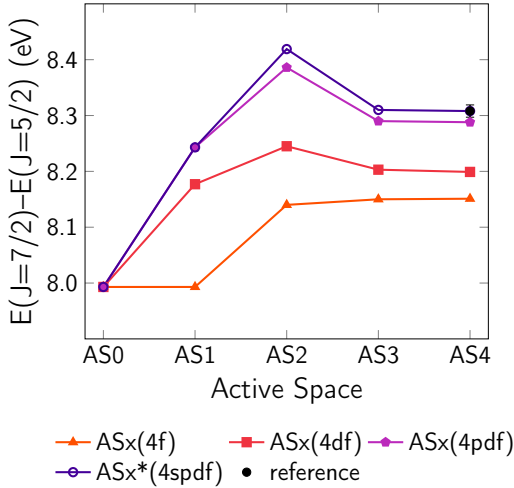


FIG. 3. Convergence of energies (in eV) for the first $J = 7/2$ atomic level in Th^{39+} , relative to the energy of the $J = 5/2$ ground state, as the active spaces used in configuration interaction calculations are extended.

tions, the radial wavefunctions were optimized separately for the $J = 5/2$ ground and $J = 7/2$ first excited states to account for the full orbital relaxation effect. The energy difference related to the frequency-dependent Breit term on energy levels has been examined at the MR level and found to be 4 meV. This value has been added to the numbers obtained for higher active spaces. Fig. 3 presents the $J = 7/2 \rightarrow J = 5/2$ transition energies, which range from about 8.0 eV to 8.4 eV, depending on the size of the active space and the number of $4l$ occupied active orbitals used in the calculations. As seen in the figure, the use of more $4l$ occupied active orbitals in the MCDF-CI calculations results in a higher transition energy. A significant increase in the transition energy for AS1 and AS2 active spaces (except for AS1(4f)) is also clearly visible. For the ASx(4f), ASx(4df), and ASx(4pdf) estimates of the $J = 7/2 \rightarrow J = 5/2$ transition energy, it is evident that the AS4 stage is adequate to achieve level energy convergence. Due to computational limitations (specifically, the limitations of the parallel RCI procedure implemented in the GRASP2018 code), we did not perform calculations at the AS3(4spdf) and AS4(4spdf) stages. Instead of the full ASx(4spdf) active space, which accounts for double virtual excitations for all 4s, 4p, 4d, and 4f subshells, we used the slightly reduced ASx*(4spdf) active space. This space contains the double virtual excitations of the 4p, 4d, and 4f subshells, along with single excitations from the 4s subshell. The difference in transition energy calculated at the AS2(4spdf) and AS2*(4spdf) stages is 11 meV. We assume that this value corresponds to the error in approximating the AS4(4spdf) value with the AS4*(4spdf) value, i.e., $\delta_{\text{approx}} = |E^{\text{AS2}(4\text{spdf})} - E^{\text{AS2}*(4\text{spdf})}|$. The uncertainty related to convergence with the size of the basis set is estimated as $\delta_{\text{conv}} = |E^{\text{AS4}*(4\text{spdf})} - E^{\text{AS3}*(4\text{spdf})}|$.

This estimation yields 2 meV. Based on the small difference between ASx(4pdf) and ASx(4spdf)/ASx*(4spdf) results, we assume that the missing correlation contributions resulting from excitations from core K , L , and M shells are negligible. The total theoretical uncertainty for the $J = 7/2 \rightarrow J = 5/2$ transition energy is then $\delta = \sqrt{(\delta_{\text{approx}})^2 + (\delta_{\text{conv}})^2} = 11$ meV. The reference value of the $J = 7/2 \rightarrow J = 5/2$ transition energy resulting from our approach is 8.308 ± 0.011 eV.

Based on the calculated energy levels, we consider the NEET mechanism for the excitation of the nuclear ground state ($5/2^+$) to the isomeric state ($3/2^+$) in Th^{39+} ions. The ground state electronic transition $|i\rangle \rightarrow |f\rangle$ is a part of a cascade decay of low-energy atomic states in Th^{39+} ions. This transition can, therefore, spontaneously induce a NEET process from the nuclear ground state to the ^{229m}Th isomer (i.e., nuclear excitation $|G\rangle \rightarrow |M\rangle$). The general expression for the probability of the NEET process, W_{NEET} , can be found in Refs. [30–32]. Assuming that $|i\rangle$ and $|f\rangle$ are the initial (upper) and final (lower) electronic states of interest and $|G\rangle$ and $|M\rangle$ are the ground and metastable (isomeric) nuclear states, the rate of the spontaneous NEET process is expressed (in atomic units) as:

$$W_{\text{NEET}} =$$

$$\frac{4\pi(\Gamma_i + \Gamma_f + \Gamma_M)}{(E_{if} - E_{GM})^2 + \frac{1}{4}(\Gamma_i + \Gamma_f + \Gamma_M)^2} \times \sum_{\lambda L} \left(\frac{E_{GM}}{c} \right)^{2L+2} \frac{(j_i \frac{1}{2} L 0 | j_f \frac{1}{2})^2}{[(2L+1)!!]^2} |M_{if}(\lambda L)|^2 B_{GM}(\lambda L), \quad (1)$$

where $\Gamma_i/\Gamma_f/\Gamma_M$ are the natural widths of the electronic and nuclear levels, $M(\lambda L)$ is the radial matrix element related to the 2^L -pole atomic transition (EL or ML) (see, e.g., [30–32] for details), $(j_i \frac{1}{2} L 0 | j_f \frac{1}{2})$ is the Clebsch-Gordan coefficient (j_i and j_f are quantum numbers for the orbitals involved in the electronic transition – $4f_{5/2}$ and $4f_{7/2}$ in our case), and E_{if} is the electronic transition energy. $B_{GM}(\lambda L)$ is the reduced probability of the nuclear transition of the type λ and multipolarity L (M1 or E2 in our case, so $L = 1, 2$), and E_{GM} is the nuclear transition energy. Note that $B_{GM}(\lambda L) = \frac{(2I_N+1)}{(2I_M+1)} B_{MG}$. The probability of a nuclear transition into an excited state during the decay of an excited atomic level $|i\rangle$ is given by $P_{\text{NEET}} = W_{\text{NEET}}/\Gamma_i$. The enhancement factor β [14, 16], which is independent of the nuclear transition probability (a major source of uncertainty in calculating W_{NEET}), is defined as $\beta = W_{\text{NEET}}/\Gamma_M$, where Γ_M is the width of the excited metastable nuclear level. The width of the nuclear level Γ_M , which is the sum of the radiative transitions (M1 and E2) between the isomeric state $|M\rangle$ and the ground state $|G\rangle$ in the ^{229}Th nucleus, is defined

(in atomic units) as [33]:

$$\Gamma_M = \sum_{\lambda L} \frac{8\pi(L+1)}{L[(2L+1)!!]^2} \left(\frac{E_{GM}}{c} \right)^{2L+1} B_{MG}(\lambda L). \quad (2)$$

The NEET process has a resonant character, and its rate is strongly dependent on the value of $\Delta = (E_{if} - E_{GM})$, where E_{if} is the energy of the electronic transition that facilitates the nuclear transition of energy E_{GM} . For this reason, an effort was made to identify an electronic transition in the Th ion with energy as close as possible to the nuclear excitation energy. The atomic state $|i\rangle$ can de-excite via an M1 or E2 transition to the ground atomic state, labeled $|f\rangle$. The $|i\rangle \rightarrow |f\rangle$ rate for the M1 transition is $1.3 \times 10^4 \text{ s}^{-1}$, while for the E2 transition, it is $1.1 \times 10^{-2} \text{ s}^{-1}$. The natural width of the $|i\rangle$ level is $8.7 \times 10^{-12} \text{ eV}$, while the natural width of the $|f\rangle$ level is effectively zero.

TABLE II. W_{NEET} (in s^{-1}), P_{NEET} , β_{NEET} , and \tilde{W}_{NEET} for various values of $|\Delta| = |E_{if} - E_{GM}|$.

$ \Delta $ (meV)	W_{NEET} (s^{-1})	P_{NEET}	β_{NEET}	\tilde{W}_{NEET} (s^{-1})
0	1.05×10^{16}	7.95×10^{11}	1.15×10^{20}	6.30×10^{19}
28	2.54×10^{-4}	1.92×10^{-8}	2.84	1.52
30	2.21×10^{-4}	1.67×10^{-8}	2.42	1.33
65	4.70×10^{-5}	3.56×10^{-9}	5.11×10^{-1}	2.82×10^{-1}
209	4.55×10^{-6}	3.44×10^{-10}	5.42×10^{-2}	5.42×10^{-2}

The values of the quantities W_{NEET} , P_{NEET} , and β_{NEET} for various values of $|\Delta| = |E_{if} - E_{GM}|$ are summarized in Table II. The calculated values of $|M_{if}(M1)|^2$ and $|M_{if}(E2)|^2$ are $3.29 \times 10^9 \text{ a.u.}$ and $4.68 \times 10^{20} \text{ a.u.}$, respectively. The probabilities of nuclear transitions are taken from Ref. [34] and are $B_{M \rightarrow G}(M1) = 0.005 \text{ W.u.}$ and $B_{M \rightarrow G}(E2) = 29 \text{ W.u.}$, respectively. Notably, the E2 excitation accounts for 94% of the NEET rate, while the M1 excitation contributes only 6%. This dominance of the E2 channel over the M1 channel has also been observed in some electronic transitions in neutral atoms and low-charged ^{229}Th ions, as reported in Ref. [35]. In Table II, the $|\Delta| = 0$ value corresponds to the NEET resonance, where the electronic transition energy E_{if} matches the nuclear transition energy E_{GM} . At resonance, the excitation rate of the ^{229m}Th isomer reaches a remarkable value of $1.05 \times 10^{16} \text{ s}^{-1}$. For non-zero Δ values, the NEET probability in Th^{39+} ions decreases by many orders of magnitude, as illustrated in Fig. 4. The other $|\Delta|$ values are chosen based on E_{GM} values from Ref. [11] (the most recent experiment where ^{229m}Th ions were incorporated into CaF_2 and MgF_2 crystals) and Ref. [8] (a previous experiment with free ^{229m}Th ions). The $|\Delta| = 28 \text{ meV}$ case refers to when E_{if} and E_{GM} from Ref. [8] are in the middle of their uncertainty intervals, with $E_{if} = 8.308 \text{ eV}$ and $E_{GM} = 8.28 \text{ eV}$. The $|\Delta| = 30 \text{ meV}$ case refers to when E_{if} and E_{GM} from Ref. [11] are in the middle of their uncertainty intervals, with $E_{if} = 8.338 \text{ eV}$ and $E_{GM} = 8.338 \text{ eV}$. The $|\Delta| = 65 \text{ meV}$ case refers to the maximum distance between E_{if} and E_{GM} according to the uncertainties from Ref. [11], with $E_{if} = (8.308 - 0.011) \text{ eV}$ and $E_{GM} = (8.338 + 0.024) \text{ eV}$. The $|\Delta| = 209 \text{ meV}$ case refers to the maximum distance between E_{if} and E_{GM} according to the uncertainties from Ref. [8], with $E_{if} = (8.308 + 0.011) \text{ eV}$ and $E_{GM} = (8.28 - 0.17) \text{ eV}$. For these Δ values, the NEET probability decreases further to $4.70 \times 10^{-5} \text{ s}^{-1}$ and $4.55 \times 10^{-6} \text{ s}^{-1}$, respectively. Given that the NEET probability changes by over 20 orders of magnitude within the uncertainty range of atomic and

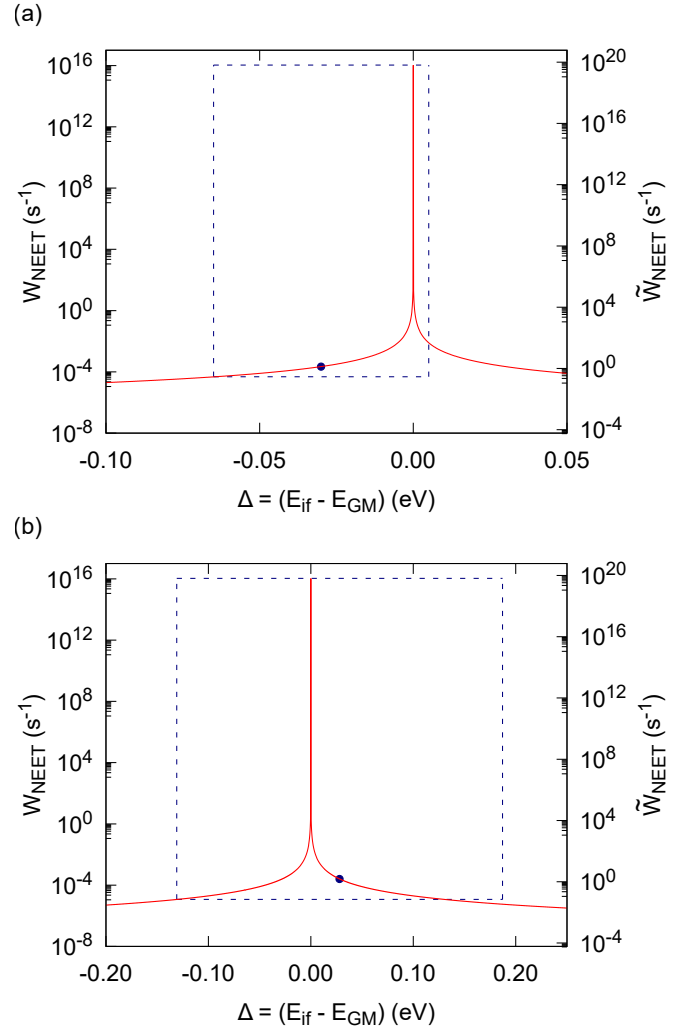


FIG. 4. Possible values of the quantities W_{NEET} and \tilde{W}_{NEET} (in s^{-1}) for various values of $\Delta = (E_{if} - E_{GM})$. The dot marks the Δ value for which both E_{if} and E_{GM} are at the center of their uncertainty intervals. The dashed box delineates the possible values of Δ and W_{NEET} based on the uncertainty intervals of the present calculated E_{if} and E_{GM} taken from: (a) Ref. [11] and (b) Ref. [8].

when E_{if} and E_{GM} from Ref. [11] are in the middle of their uncertainty intervals, with $E_{if} = 8.308 \text{ eV}$ and $E_{GM} = 8.338 \text{ eV}$. For these Δ values, the NEET probability decreases to $2.54 \times 10^{-4} \text{ s}^{-1}$ and $2.21 \times 10^{-4} \text{ s}^{-1}$, respectively. The $|\Delta| = 65 \text{ meV}$ case refers to the maximum distance between E_{if} and E_{GM} according to the uncertainties from Ref. [11], with $E_{if} = (8.308 - 0.011) \text{ eV}$ and $E_{GM} = (8.338 + 0.024) \text{ eV}$. The $|\Delta| = 209 \text{ meV}$ case refers to the maximum distance between E_{if} and E_{GM} according to the uncertainties from Ref. [8], with $E_{if} = (8.308 + 0.011) \text{ eV}$ and $E_{GM} = (8.28 - 0.17) \text{ eV}$. For these Δ values, the NEET probability decreases further to $4.70 \times 10^{-5} \text{ s}^{-1}$ and $4.55 \times 10^{-6} \text{ s}^{-1}$, respectively. Given that the NEET probability changes by over 20 orders of magnitude within the uncertainty range of atomic and

nuclear transition energies, the NEET process in Th^{39+} ions represents an extremely sensitive tool for verifying the excitation energy of the ^{229m}Th isomer.

To estimate the isomeric excitation rate in Th^{39+} ions achievable in an EBIT device, we assumed experimental conditions similar to those described in Ref. [17]. Specifically, we considered an ion cloud with a diameter of $100\text{ }\mu\text{m}$ containing approximately $N_{\text{HCl}} \simeq 10^6$ Th^{39+} ions. Such a large number of exotic HCIs can be produced in an EBIT using a highly efficient technique based on in-trap laser-induced desorption of atoms from a sample positioned near the electron beam [36]. Our collisional-radiative model simulations, conducted using the FAC code [37], indicate that the relative steady-state population of the first excited $J = 7/2$ level in Th^{39+} ions is about $p_i \simeq 0.6\%$ at an electron temperature of 2 keV in the EBIT. Details of these simulations are provided in the Supplementary Material. The NEET rate achievable in the EBIT device is then calculated as $\tilde{W}_{\text{NEET}} = W_{\text{NEET}} \cdot p_i \cdot N_{\text{HCl}}$. Possible values of \tilde{W}_{NEET} as a function of the energy difference $|\Delta| = |E_{if} - E_{GM}|$ are presented in Table II and Fig. 4 (refer to the scale on the right side of the figure). At resonance ($|\Delta| = 0$), the upper limit of the NEET isomeric excitation rate in the ^{229}Th nucleus under EBIT conditions reaches an enormous value of $6.30 \times 10^{19}\text{ s}^{-1}$, which is several orders of magnitude higher than the maximum rate (just over 10^5 s^{-1}) achievable using the EBE mechanism in Th^{35+} ions, as described in Ref. [17]. Within the energy uncertainty range of the nuclear and atomic transitions, the NEET rate under EBIT conditions decreases to $2.82 \times 10^{-1}\text{ s}^{-1}$ for $|\Delta| = 65\text{ meV}$ and to $5.42 \times 10^{-2}\text{ s}^{-1}$ for $|\Delta| = 209\text{ meV}$. While these lower NEET rates are two orders of magnitude below the lower limit observed for the EBE mechanism in $^{229}\text{Th}^{35+}$ ions, they still appear to be detectable in spectroscopy measurements of the internal conversion electrons emitted during the isomer decay from neutralized ^{229m}Th ions [17]. Furthermore, our proposed experimental scenario eliminates the need for a tunable UV laser to initiate the atomic and nuclear processes, which significantly simplifies the experimental setup.

In summary, the NEET excitation of the ^{229m}Th isomer has been theoretically investigated for highly charged thorium ions. It was found that the atomic transition energy from the first excited state to the ground state in $^{229}\text{Th}^{39+}$ ions ($8.308 \pm 0.011\text{ eV}$) closely matches the newly established experimental reference value for the nuclear isomer excitation energy ($8.338 \pm 0.024\text{ eV}$). The study demonstrated that NEET can produce the isomeric state in the ^{229}Th nucleus at rates reaching up to 10^{16} s^{-1} . Moreover, the NEET probabilities vary by over 20 orders of magnitude within the uncertainty ranges of the atomic and nuclear transition energies. General calculations for the experimental scenario in the EBIT facility were also performed. Within the range of energy uncertainties of nuclear and atomic transitions, NEET rates for EBIT

conditions range from 0.05 s^{-1} to $6.3 \times 10^{19}\text{ s}^{-1}$ at resonance. Thus, the NEET process in $^{229}\text{Th}^{39+}$ ions could be a unique opportunity to efficiently produce the ^{229m}Th isomer in the EBIT facility as well as for a rigorous test of its excitation energy.

* Karol.Koziol@ncbj.gov.pl

† Jacek.Rzadkiewicz@ncbj.gov.pl

- [1] C. J. Campbell, A. G. Radnaev, A. Kuzmich, V. A. Dzuba, V. V. Flambaum, and A. Derevianko, *Physical Review Letters* **108**, 120802 (2012).
- [2] E. Peik, T. Schumm, M. S. Safranova, A. Pálffy, J. Weitenberg, and P. G. Thirolf, *Quantum Science and Technology* **6**, 034002 (2021).
- [3] K. Beeks, T. Sikorsky, T. Schumm, J. Thielking, M. V. Okhapkin, and E. Peik, *Nature Reviews Physics* **3**, 238 (2021).
- [4] V. V. Flambaum, *Physical Review Letters* **97**, 092502 (2006).
- [5] J. C. Berengut, V. A. Dzuba, V. V. Flambaum, and S. G. Porsev, *Physical Review Letters* **102**, 210801 (2009).
- [6] P. G. Thirolf, B. Seiferle, and L. von der Wense, *Annalen der Physik* **531**, 1800381 (2019).
- [7] J. Tiedau, M. V. Okhapkin, K. Zhang, J. Thielking, G. Zitter, E. Peik, F. Schaden, T. Pronebner, I. Morawetz, L. T. De Col, F. Schneider, A. Leitner, M. Pressler, G. A. Kazakov, K. Beeks, T. Sikorsky, and T. Schumm, *Physical Review Letters* **132**, 182501 (2024).
- [8] B. Seiferle, L. von der Wense, P. V. Bilous, I. Amersdorffer, C. Lemell, F. Libisch, S. Stellmer, T. Schumm, C. E. Düllmann, A. Pálffy, and P. G. Thirolf, *Nature* **573**, 243 (2019).
- [9] A. Yamaguchi, H. Muramatsu, T. Hayashi, N. Yuasa, K. Nakamura, M. Takimoto, H. Haba, K. Konashi, M. Watanabe, H. Kikunaga, K. Maehata, N. Y. Yamasaki, and K. Mitsuda, *Physical Review Letters* **123**, 222501 (2019).
- [10] T. Sikorsky, J. Geist, D. Hengstler, S. Kempf, L. Gastaldo, C. Enss, C. Mokry, J. Runke, C. E. Düllmann, P. Wobrabschek, K. Beeks, V. Rosecker, J. H. Sterba, G. Kazakov, T. Schumm, and A. Fleischmann, *Physical Review Letters* **125**, 142503 (2020).
- [11] S. Kraemer, J. Moens, M. Athanasakis-Kaklamanakis, S. Bara, K. Beeks, P. Chhetri, K. Chrysalidis, A. Claessens, T. E. Cocolios, J. G. M. Correia, H. D. Witte, R. Ferrer, S. Geldhof, R. Heinke, N. Hosseini, M. Huyse, U. Köster, Y. Kudryavtsev, M. Laatiaoui, R. Lica, G. Magchiels, V. Manea, C. Merckling, L. M. C. Pereira, S. Raeder, T. Schumm, S. Sels, P. G. Thirolf, S. M. Tunhuma, P. Van Den Bergh, P. Van Duppen, A. Vantomme, M. Verlinde, R. Villarreal, and U. Wahl, *Nature* **617**, 706 (2023).
- [12] T. Masuda, A. Yoshimi, A. Fujieda, H. Fujimoto, H. Haba, H. Hara, T. Hiraki, H. Kaino, Y. Kasamatsu, S. Kitao, K. Konashi, Y. Miyamoto, K. Okai, S. Okubo, N. Sasao, M. Seto, T. Schumm, Y. Shigekawa, K. Suzuki, S. Stellmer, K. Tamasaku, S. Uetake, M. Watanabe, T. Watanabe, Y. Yasuda, A. Yamaguchi, Y. Yoda, T. Yokokita, M. Yoshimura, and K. Yoshimura, *Nature* **573**, 238 (2019).

- [13] J. Zhao, A. Pálffy, C. H. Keitel, and Y. Wu, *Physical Review C* **110**, 014330 (2024).
- [14] S. G. Porsev and V. V. Flambaum, *Physical Review A* **81**, 032504 (2010).
- [15] S. G. Porsev, V. V. Flambaum, E. Peik, and C. Tamm, *Physical Review Letters* **105**, 182501 (2010).
- [16] R. A. Müller, A. V. Volotka, and A. Surzhykov, *Physical Review A* **99**, 042517 (2019).
- [17] P. V. Bilous, H. Bekker, J. C. Berengut, B. Seiferle, L. von der Wense, P. G. Thirolf, T. Pfeifer, J. R. C. López-Urrutia, and A. Pálffy, *Physical Review Letters* **124**, 192502 (2020).
- [18] B. S. Nickerson, M. Pimon, P. V. Bilous, J. Gugler, K. Beeks, T. Sikorsky, P. Mohn, T. Schumm, and A. Pálffy, *Physical Review Letters* **125**, 032501 (2020).
- [19] S. G. Porsev and V. V. Flambaum, *Physical Review A* **81**, 042516 (2010).
- [20] H. Zhang and X. Wang, *Frontiers in Physics* **11**, 1 (2023).
- [21] E. Peik and M. Okhapkin, *Comptes Rendus Physique* **16**, 516 (2015).
- [22] S. G. Porsev, C. Cheung, and M. S. Safronova, *Quantum Science and Technology* **6**, 034014 (2021).
- [23] C. Froese Fischer, G. Gaigalas, P. Jönsson, and J. Bieroń, *Computer Physics Communications* **237**, 184 (2019).
- [24] I. P. Grant, *Relativistic Quantum Theory of Atoms and Molecules*, edited by I. P. Grant, Springer Series on Atomic, Optical, and Plasma Physics, Vol. 40 (Springer, New York, NY, 2007).
- [25] C. Froese Fischer, M. R. Godefroid, T. Brage, P. Jönsson, and G. Gaigalas, *Journal of Physics B: Atomic, Molecular and Optical Physics* **49**, 182004 (2016).
- [26] K. Kozioł and J. Rzadkiewicz, *Physical Review A* **98**, 062504 (2018).
- [27] I. P. Grant, *International Journal of Quantum Chemistry* **25**, 23 (1984).
- [28] R. Si, X. L. Guo, T. Brage, C. Y. Chen, R. Hutton, and C. Froese Fischer, *Physical Review A* **98**, 012504 (2018).
- [29] W. Li, J. Grumer, T. Brage, and P. Jönsson, *Computer Physics Communications* **253**, 107211 (2020).
- [30] E. V. Tkalya, *Nuclear Physics A* **539**, 209 (1992).
- [31] M. Harston, *Nuclear Physics A* **690**, 447 (2001).
- [32] D. Denis-Petit, G. Gosselin, F. Hannachi, M. Tarisien, T. Bonnet, M. Comet, F. Gobet, M. Versteegen, P. Morel, V. Méot, and I. Matea, *Physical Review C* **96**, 024604 (2017).
- [33] P. Ring and P. Schuck, *The Nuclear Many-Body Problem* (Springer-Verlag, 1980).
- [34] N. Minkov and A. Pálffy, *Physical Review Letters* **122**, 162502 (2019).
- [35] P. V. Bilous, N. Minkov, and A. Pálffy, *Physical Review C* **97**, 044320 (2018).
- [36] C. Schweiger, C. M. König, J. R. Crespo López-Urrutia, M. Door, H. Dorrer, C. E. Düllmann, S. Eliseev, P. Filianin, W. Huang, K. Kromer, P. Micke, M. Müller, D. Renisch, A. Rischka, R. X. Schüssler, and K. Blaum, *Review of Scientific Instruments* **90**, 123201 (2019).
- [37] M. F. Gu, *Canadian Journal of Physics* **86**, 675 (2008).

Nuclear Excitation by Near-Resonant Electron Transition in $^{229}\text{Th}^{39+}$ Ions – Supplementary Material

Karol Kozioł* and Jacek Rzadkiewicz†

Narodowe Centrum Badań Jądrowych (NCBJ), Andrzeja Soltana 7, 05-400 Otwock-Świerk, Poland

ENERGIES OF ALL $[\text{Kr}]4\text{d}^{10}4\text{f}^5$ LEVELS IN Th^{39+}

Table I lists the energies and LS -compositions of all $[\text{Kr}]4\text{d}^{10}4\text{f}^5$ levels, calculated at the AS2(4df) level of theory. The energy uncertainties are approximately 0.2 eV for states below 16 eV, 0.5 eV for states in the range 16 eV to 60 eV, 1 eV for states in the range 60 eV to 80 eV, and 2 eV for states above 80 eV.

A graphical representation of the level arrangement is presented in Figure 1.

TABLE I: Energies of all $[\text{Kr}]4\text{d}^{10}4\text{f}^5$ levels in Th^{39+} .

No.	J	LS -composition	E (cm^{-1})	E (eV)
1	5/2	$0.27 4d^{10}(^1S)4f^5(^6H) ^6H + 0.18 4d^{10}(^1S)4f^5(^4G) ^4G + 0.15 4d^{10}(^1S)4f^5(^4G) ^4G$	0	0.000
2	7/2	$0.53 4d^{10}(^1S)4f^5(^6H) ^6H + 0.17 4d^{10}(^1S)4f^5(^4G) ^4G + 0.13 4d^{10}(^1S)4f^5(^4G) ^4G$	65 541	8.126
3	5/2	$0.31 4d^{10}(^1S)4f^5(^6H) ^6H + 0.16 4d^{10}(^1S)4f^5(^6F) ^6F + 0.08 4d^{10}(^1S)4f^5(^3F) ^4F$	78 003	9.671
4	3/2	$0.40 4d^{10}(^1S)4f^5(^6F) ^6F + 0.23 4d^{10}(^1S)4f^5(^4F) ^4F + 0.07 4d^{10}(^1S)4f^5(^4F) ^4F$	83 788	10.388
5	1/2	$0.52 4d^{10}(^1S)4f^5(^6F) ^6F + 0.12 4d^{10}(^1S)4f^5(^4D) ^4D + 0.10 4d^{10}(^1S)4f^5(^4D) ^4D$	94 082	11.665
6	9/2	$0.48 4d^{10}(^1S)4f^5(^6H) ^6H + 0.10 4d^{10}(^1S)4f^5(^3I) ^4I + 0.06 4d^{10}(^1S)4f^5(^4G) ^4G$	100 531	12.464
7	15/2	$0.21 4d^{10}(^1S)4f^5(^4M) ^4M + 0.17 4d^{10}(^1S)4f^5(^2L) ^2L + 0.12 4d^{10}(^1S)4f^5(^4I) ^4I$	107 412	13.317
8	11/2	$0.28 4d^{10}(^1S)4f^5(^6H) ^6H + 0.14 4d^{10}(^1S)4f^5(^4I) ^4I + 0.12 4d^{10}(^1S)4f^5(^4K) ^4K$	115 286	14.294
9	7/2	$0.34 4d^{10}(^1S)4f^5(^6F) ^6F + 0.14 4d^{10}(^1S)4f^5(^6H) ^6H + 0.12 4d^{10}(^1S)4f^5(^4F) ^4F$	120 776	14.974
10	13/2	$0.17 4d^{10}(^1S)4f^5(^4I) ^4I + 0.17 4d^{10}(^1S)4f^5(^4L) ^4L + 0.15 4d^{10}(^1S)4f^5(^6H) ^6H$	121 603	15.077
11	9/2	$0.23 4d^{10}(^1S)4f^5(^6F) ^6F + 0.14 4d^{10}(^1S)4f^5(^6H) ^6H + 0.09 4d^{10}(^1S)4f^5(^3G) ^4G$	141 565	17.552
12	5/2	$0.35 4d^{10}(^1S)4f^5(^6F) ^6F + 0.17 4d^{10}(^1S)4f^5(^2P) ^4P + 0.11 4d^{10}(^1S)4f^5(^6P) ^6P$	157 053	19.472
13	11/2	$0.17 4d^{10}(^1S)4f^5(^6F) ^6F + 0.17 4d^{10}(^1S)4f^5(^6H) ^6H + 0.15 4d^{10}(^1S)4f^5(^4G) ^4G$	162 253	20.117
14	9/2	$0.25 4d^{10}(^1S)4f^5(^4I) ^4I + 0.15 4d^{10}(^1S)4f^5(^6H) ^6H + 0.12 4d^{10}(^1S)4f^5(^6F) ^6F$	169 886	21.063
15	5/2	$0.22 4d^{10}(^1S)4f^5(^6H) ^6H + 0.13 4d^{10}(^1S)4f^5(^6F) ^6F + 0.09 4d^{10}(^1S)4f^5(^6P) ^6P$	171 184	21.224
16	15/2	$0.33 4d^{10}(^1S)4f^5(^4M) ^4M + 0.26 4d^{10}(^1S)4f^5(^6H) ^6H + 0.23 4d^{10}(^1S)4f^5(^4I) ^4I$	174 999	21.697
17	3/2	$0.33 4d^{10}(^1S)4f^5(^6F) ^6F + 0.32 4d^{10}(^1S)4f^5(^4F) ^4F + 0.09 4d^{10}(^1S)4f^5(^4F) ^4F$	176 628	21.899
18	11/2	$0.28 4d^{10}(^1S)4f^5(^4K) ^4K + 0.27 4d^{10}(^1S)4f^5(^6H) ^6H + 0.10 4d^{10}(^1S)4f^5(^6F) ^6F$	178 909	22.182
19	13/2	$0.38 4d^{10}(^1S)4f^5(^6H) ^6H + 0.36 4d^{10}(^1S)4f^5(^4L) ^4L + 0.07 4d^{10}(^1S)4f^5(^4I) ^4I$	181 751	22.534
20	3/2	$0.30 4d^{10}(^1S)4f^5(^6P) ^6P + 0.28 4d^{10}(^1S)4f^5(^2P) ^4P + 0.07 4d^{10}(^1S)4f^5(^2D) ^2D$	183 329	22.730
21	1/2	$0.32 4d^{10}(^1S)4f^5(^6F) ^6F + 0.31 4d^{10}(^1S)4f^5(^4P) ^2P + 0.20 4d^{10}(^1S)4f^5(^3P) ^2P$	187 634	23.264
22	17/2	$0.56 4d^{10}(^1S)4f^5(^4M) ^4M + 0.18 4d^{10}(^1S)4f^5(^4L) ^4L + 0.13 4d^{10}(^1S)4f^5(^2L) ^2L$	192 130	23.821
23	7/2	$0.23 4d^{10}(^1S)4f^5(^6F) ^6F + 0.18 4d^{10}(^1S)4f^5(^4H) ^4H + 0.17 4d^{10}(^1S)4f^5(^4H) ^4H$	193 852	24.035
24	7/2	$0.22 4d^{10}(^1S)4f^5(^2G) ^4G + 0.16 4d^{10}(^1S)4f^5(^6H) ^6H + 0.10 4d^{10}(^1S)4f^5(^4G) ^4G$	200 513	24.860
25	9/2	$0.26 4d^{10}(^1S)4f^5(^6F) ^6F + 0.23 4d^{10}(^1S)4f^5(^4I) ^4I + 0.11 4d^{10}(^1S)4f^5(^2H) ^2H$	211 314	26.200
26	15/2	$0.51 4d^{10}(^1S)4f^5(^4L) ^4L + 0.14 4d^{10}(^1S)4f^5(^4K) ^4K + 0.10 4d^{10}(^1S)4f^5(^2K) ^4K$	212 502	26.347

TABLE I: Continued.

No.	J	LS-composition	E (cm ⁻¹)	E (eV)
27	9/2	0.22 $4d^{10}(^1_0S) 4f^5(^4_1H) ^4H + 0.20 4d^{10}(^1_0S) 4f^5(^4_2G) ^4G + 0.10 4d^{10}(^1_0S) 4f^5(^4_1I) ^4I$	212 855	26.391
28	19/2	0.39 $4d^{10}(^1_0S) 4f^5(^4_0M) ^4M + 0.30 4d^{10}(^1_0S) 4f^5(^2_1N) ^2N + 0.15 4d^{10}(^1_0S) 4f^5(^4_1L) ^4L$	214 609	26.608
29	5/2	0.17 $4d^{10}(^1_0S) 4f^5(^2_4D) ^2D + 0.13 4d^{10}(^1_0S) 4f^5(^4_2D) ^4D + 0.11 4d^{10}(^1_0S) 4f^5(^2_4F) ^2F$	217 471	26.963
30	21/2	0.45 $4d^{10}(^1_0S) 4f^5(^2_1N) ^2N + 0.29 4d^{10}(^1_0S) 4f^5(^4_0M) ^4M + 0.26 4d^{10}(^1_0S) 4f^5(^2_0O) ^2O$	218 770	27.124
31	11/2	0.19 $4d^{10}(^1_0S) 4f^5(^4_1H) ^4H + 0.11 4d^{10}(^1_0S) 4f^5(^4_2I) ^4I + 0.11 4d^{10}(^1_0S) 4f^5(^6_0F) ^6F$	219 853	27.258
32	17/2	0.41 $4d^{10}(^1_0S) 4f^5(^2_2M) ^2M + 0.24 4d^{10}(^1_0S) 4f^5(^4_1L) ^4L + 0.14 4d^{10}(^1_0S) 4f^5(^2_2L) ^2L$	222 937	27.641
33	13/2	0.51 $4d^{10}(^1_0S) 4f^5(^4_1K) ^4K + 0.09 4d^{10}(^1_0S) 4f^5(^2_3K) ^2K + 0.09 4d^{10}(^1_0S) 4f^5(^2_4I) ^2I$	223 227	27.677
34	3/2	0.24 $4d^{10}(^1_0S) 4f^5(^4_1P) ^4P + 0.13 4d^{10}(^1_0S) 4f^5(^2_3D) ^2D + 0.10 4d^{10}(^1_0S) 4f^5(^4_2D) ^4D$	225 076	27.906
35	13/2	0.25 $4d^{10}(^1_0S) 4f^5(^4_2I) ^4I + 0.14 4d^{10}(^1_0S) 4f^5(^4_1H) ^4H + 0.14 4d^{10}(^1_0S) 4f^5(^2_5K) ^2K$	227 535	28.211
36	5/2	0.25 $4d^{10}(^1_0S) 4f^5(^4_3F) ^4F + 0.18 4d^{10}(^1_0S) 4f^5(^4_3G) ^4G + 0.13 4d^{10}(^1_0S) 4f^5(^4_4F) ^4F$	230 234	28.545
37	7/2	0.30 $4d^{10}(^1_0S) 4f^5(^6_0P) ^6P + 0.21 4d^{10}(^1_0S) 4f^5(^4_1D) ^4D + 0.10 4d^{10}(^1_0S) 4f^5(^4_2F) ^4F$	230 506	28.579
38	9/2	0.22 $4d^{10}(^1_0S) 4f^5(^4_2F) ^4F + 0.13 4d^{10}(^1_0S) 4f^5(^4_3I) ^4I + 0.10 4d^{10}(^1_0S) 4f^5(^2_3G) ^2G$	236 983	29.382
39	11/2	0.22 $4d^{10}(^1_0S) 4f^5(^6_0F) ^6F + 0.19 4d^{10}(^1_0S) 4f^5(^4_2K) ^4K + 0.12 4d^{10}(^1_0S) 4f^5(^2_4I) ^2I$	239 217	29.659
40	15/2	0.20 $4d^{10}(^1_0S) 4f^5(^4_2I) ^4I + 0.19 4d^{10}(^1_0S) 4f^5(^2_2K) ^2K + 0.16 4d^{10}(^1_0S) 4f^5(^6_0H) ^6H$	245 087	30.387
41	5/2	0.31 $4d^{10}(^1_0S) 4f^5(^6_0P) ^6P + 0.20 4d^{10}(^1_0S) 4f^5(^4_3G) ^4G + 0.11 4d^{10}(^1_0S) 4f^5(^4_2G) ^4G$	247 229	30.653
42	7/2	0.14 $4d^{10}(^1_0S) 4f^5(^4_3G) ^4G + 0.12 4d^{10}(^1_0S) 4f^5(^4_3H) ^4H + 0.09 4d^{10}(^1_0S) 4f^5(^4_1G) ^4G$	252 805	31.344
43	11/2	0.18 $4d^{10}(^1_0S) 4f^5(^6_2H) ^2H + 0.17 4d^{10}(^1_0S) 4f^5(^4_2I) ^4I + 0.14 4d^{10}(^1_0S) 4f^5(^4_2H) ^2H$	254 995	31.615
44	3/2	0.19 $4d^{10}(^1_0S) 4f^5(^6_0P) ^6P + 0.15 4d^{10}(^1_0S) 4f^5(^4_2F) ^4F + 0.14 4d^{10}(^1_0S) 4f^5(^2_3D) ^2D$	257 399	31.913
45	7/2	0.14 $4d^{10}(^1_0S) 4f^5(^6_0P) ^6P + 0.11 4d^{10}(^1_0S) 4f^5(^4_2D) ^4D + 0.09 4d^{10}(^1_0S) 4f^5(^2_5G) ^2G$	259 854	32.218
46	11/2	0.42 $4d^{10}(^1_0S) 4f^5(^4_3I) ^4I + 0.08 4d^{10}(^1_0S) 4f^5(^2_4I) ^2I + 0.08 4d^{10}(^1_0S) 4f^5(^4_4G) ^4G$	260 266	32.269
47	9/2	0.24 $4d^{10}(^1_0S) 4f^5(^4_2F) ^4F + 0.13 4d^{10}(^1_0S) 4f^5(^4_3H) ^4H + 0.10 4d^{10}(^1_0S) 4f^5(^4_2I) ^4I$	264 199	32.757
48	13/2	0.34 $4d^{10}(^1_0S) 4f^5(^6_0H) ^6H + 0.24 4d^{10}(^1_0S) 4f^5(^4_1L) ^4L + 0.12 4d^{10}(^1_0S) 4f^5(^4_2I) ^2I$	265 732	32.947
49	7/2	0.22 $4d^{10}(^1_0S) 4f^5(^4_2G) ^4G + 0.14 4d^{10}(^1_0S) 4f^5(^4_3D) ^4D + 0.13 4d^{10}(^1_0S) 4f^5(^6_0F) ^6F$	267 657	33.185
50	15/2	0.25 $4d^{10}(^1_0S) 4f^5(^6_0H) ^6H + 0.16 4d^{10}(^1_0S) 4f^5(^4_2M) ^4M + 0.13 4d^{10}(^1_0S) 4f^5(^2_2L) ^2L$	268 448	33.283
51	5/2	0.33 $4d^{10}(^1_0S) 4f^5(^4_2F) ^4F + 0.24 4d^{10}(^1_0S) 4f^5(^2_3D) ^2D + 0.12 4d^{10}(^1_0S) 4f^5(^4_1P) ^4P$	269 210	33.378
52	13/2	0.18 $4d^{10}(^1_0S) 4f^5(^4_2K) ^4K + 0.18 4d^{10}(^1_0S) 4f^5(^2_5K) ^2K + 0.17 4d^{10}(^1_0S) 4f^5(^4_2I) ^2I$	276 183	34.242
53	11/2	0.09 $4d^{10}(^1_0S) 4f^5(^2_4H) ^2H + 0.09 4d^{10}(^1_0S) 4f^5(^2_3H) ^2H + 0.09 4d^{10}(^1_0S) 4f^5(^2_6H) ^2H$	277 228	34.372
54	3/2	0.26 $4d^{10}(^1_0S) 4f^5(^4_3D) ^4D + 0.15 4d^{10}(^1_0S) 4f^5(^6_0F) ^6F + 0.15 4d^{10}(^1_0S) 4f^5(^4_1D) ^4D$	278 577	34.539
55	17/2	0.52 $4d^{10}(^1_0S) 4f^5(^4_1K) ^4K + 0.30 4d^{10}(^1_0S) 4f^5(^4_2M) ^4M + 0.06 4d^{10}(^1_0S) 4f^5(^4_1L) ^4L$	284 025	35.215
56	5/2	0.23 $4d^{10}(^1_0S) 4f^5(^4_3G) ^4G + 0.20 4d^{10}(^1_0S) 4f^5(^4_2G) ^4G + 0.17 4d^{10}(^1_0S) 4f^5(^4_3F) ^4F$	285 011	35.337
57	9/2	0.15 $4d^{10}(^1_0S) 4f^5(^4_1G) ^4G + 0.10 4d^{10}(^1_0S) 4f^5(^4_4G) ^4G + 0.09 4d^{10}(^1_0S) 4f^5(^4_3H) ^4H$	285 961	35.455
58	1/2	0.66 $4d^{10}(^1_0S) 4f^5(^4_2P) ^4P + 0.16 4d^{10}(^1_0S) 4f^5(^4_3D) ^4D + 0.05 4d^{10}(^1_0S) 4f^5(^4_1D) ^4D$	289 121	35.846
59	7/2	0.17 $4d^{10}(^1_0S) 4f^5(^4_1H) ^4H + 0.12 4d^{10}(^1_0S) 4f^5(^6_0F) ^6F + 0.11 4d^{10}(^1_0S) 4f^5(^4_3H) ^4H$	290 271	35.989
60	19/2	0.53 $4d^{10}(^1_0S) 4f^5(^4_0M) ^4M + 0.20 4d^{10}(^1_0S) 4f^5(^2_1M) ^2M + 0.15 4d^{10}(^1_0S) 4f^5(^2_1N) ^2N$	294 456	36.508
61	9/2	0.22 $4d^{10}(^1_0S) 4f^5(^4_1H) ^4H + 0.16 4d^{10}(^1_0S) 4f^5(^2_5G) ^2G + 0.15 4d^{10}(^1_0S) 4f^5(^4_2G) ^4G$	297 307	36.861
62	15/2	0.51 $4d^{10}(^1_0S) 4f^5(^4_1K) ^4K + 0.24 4d^{10}(^1_0S) 4f^5(^4_1L) ^4L + 0.07 4d^{10}(^1_0S) 4f^5(^2_5K) ^2K$	297 555	36.892
63	7/2	0.15 $4d^{10}(^1_0S) 4f^5(^6_0P) ^6P + 0.14 4d^{10}(^1_0S) 4f^5(^4_4F) ^4F + 0.11 4d^{10}(^1_0S) 4f^5(^4_2F) ^4F$	301 128	37.335

TABLE I: Continued.

No.	J	LS-composition	E (cm ⁻¹)	E (eV)
64	9/2	0.15 $4d^{10}(0S)4f^5(2I)^4I + 0.14 4d^{10}(0S)4f^5(4F)^4F + 0.10 4d^{10}(0S)4f^5(6F)^6F$	303 898	37.679
65	11/2	0.24 $4d^{10}(0S)4f^5(4G)^4G + 0.16 4d^{10}(0S)4f^5(6F)^6F + 0.13 4d^{10}(0S)4f^5(4K)^4K$	304 135	37.708
66	21/2	0.50 $4d^{10}(0S)4f^5(4M)^4M + 0.49 4d^{10}(0S)4f^5(2O)^2O$	305 062	37.823
67	19/2	0.53 $4d^{10}(0S)4f^5(4L)^4L + 0.39 4d^{10}(0S)4f^5(2N)^2N + 0.06 4d^{10}(0S)4f^5(2M)^2M$	306 697	38.026
68	13/2	0.22 $4d^{10}(0S)4f^5(4H)^4H + 0.15 4d^{10}(0S)4f^5(2K)^2K + 0.12 4d^{10}(0S)4f^5(4I)^4I$	309 276	38.345
69	1/2	0.50 $4d^{10}(0S)4f^5(4P)^4P + 0.32 4d^{10}(0S)4f^5(4D)^4D + 0.05 4d^{10}(0S)4f^5(6F)^6F$	313 235	38.836
70	17/2	0.43 $4d^{10}(0S)4f^5(2M)^2M + 0.27 4d^{10}(0S)4f^5(4L)^4L + 0.08 4d^{10}(0S)4f^5(4K)^4K$	313 543	38.874
71	3/2	0.24 $4d^{10}(0S)4f^5(4D)^4D + 0.11 4d^{10}(0S)4f^5(4F)^4F + 0.10 4d^{10}(0S)4f^5(6P)^6P$	315 440	39.110
72	5/2	0.16 $4d^{10}(0S)4f^5(3D)^4D + 0.11 4d^{10}(0S)4f^5(3D)^2D + 0.11 4d^{10}(0S)4f^5(4F)^2F$	316 602	39.254
73	7/2	0.16 $4d^{10}(0S)4f^5(3H)^4H + 0.14 4d^{10}(0S)4f^5(3D)^4D + 0.12 4d^{10}(0S)4f^5(2F)^4F$	319 409	39.602
74	11/2	0.31 $4d^{10}(0S)4f^5(3H)^4H + 0.12 4d^{10}(0S)4f^5(4G)^4G + 0.12 4d^{10}(0S)4f^5(4K)^4K$	319 805	39.651
75	9/2	0.20 $4d^{10}(0S)4f^5(3G)^4G + 0.10 4d^{10}(0S)4f^5(2G)^4G + 0.08 4d^{10}(0S)4f^5(3H)^4H$	322 151	39.942
76	5/2	0.17 $4d^{10}(0S)4f^5(2F)^4F + 0.15 4d^{10}(0S)4f^5(6P)^6P + 0.14 4d^{10}(0S)4f^5(4P)^4P$	326 660	40.501
77	13/2	0.21 $4d^{10}(0S)4f^5(5K)^2K + 0.20 4d^{10}(0S)4f^5(3H)^4H + 0.17 4d^{10}(0S)4f^5(3K)^2K$	326 936	40.535
78	17/2	0.30 $4d^{10}(0S)4f^5(2K)^4K + 0.24 4d^{10}(0S)4f^5(3L)^2L + 0.19 4d^{10}(0S)4f^5(2M)^2M$	329 178	40.813
79	11/2	0.16 $4d^{10}(0S)4f^5(4I)^4I + 0.15 4d^{10}(0S)4f^5(4H)^2H + 0.14 4d^{10}(0S)4f^5(4H)^4H$	329 877	40.900
80	7/2	0.24 $4d^{10}(0S)4f^5(2H)^4H + 0.13 4d^{10}(0S)4f^5(4F)^4F + 0.10 4d^{10}(0S)4f^5(3H)^4H$	330 821	41.017
81	15/2	0.44 $4d^{10}(0S)4f^5(2I)^4I + 0.25 4d^{10}(0S)4f^5(2L)^2L + 0.09 4d^{10}(0S)4f^5(1L)^2L$	331 886	41.149
82	5/2	0.15 $4d^{10}(0S)4f^5(3D)^4D + 0.13 4d^{10}(0S)4f^5(4P)^4P + 0.10 4d^{10}(0S)4f^5(3G)^4G$	334 913	41.524
83	23/2	0.99 $4d^{10}(0S)4f^5(2O)^2O$	335 551	41.603
84	11/2	0.20 $4d^{10}(0S)4f^5(3G)^4G + 0.09 4d^{10}(0S)4f^5(5H)^2H + 0.07 4d^{10}(0S)4f^5(4K)^4K$	337 400	41.832
85	3/2	0.15 $4d^{10}(0S)4f^5(2F)^4F + 0.15 4d^{10}(0S)4f^5(6P)^6P + 0.11 4d^{10}(0S)4f^5(1S)^4S$	338 191	41.930
86	13/2	0.29 $4d^{10}(0S)4f^5(2I)^4I + 0.17 4d^{10}(0S)4f^5(1H)^4H + 0.11 4d^{10}(0S)4f^5(1I)^2I$	338 913	42.020
87	7/2	0.33 $4d^{10}(0S)4f^5(3G)^2G + 0.08 4d^{10}(0S)4f^5(6G)^2G + 0.08 4d^{10}(0S)4f^5(1H)^4H$	342 206	42.428
88	9/2	0.19 $4d^{10}(0S)4f^5(3G)^2G + 0.18 4d^{10}(0S)4f^5(3H)^2H + 0.16 4d^{10}(0S)4f^5(4F)^4F$	343 071	42.535
89	15/2	0.37 $4d^{10}(0S)4f^5(2K)^4K + 0.17 4d^{10}(0S)4f^5(3L)^2L + 0.12 4d^{10}(0S)4f^5(3I)^4I$	343 380	42.574
90	3/2	0.22 $4d^{10}(0S)4f^5(5D)^2D + 0.13 4d^{10}(0S)4f^5(1P)^4P + 0.10 4d^{10}(0S)4f^5(2D)^2D$	345 345	42.817
91	7/2	0.31 $4d^{10}(0S)4f^5(3F)^2F + 0.15 4d^{10}(0S)4f^5(4F)^4F + 0.10 4d^{10}(0S)4f^5(3F)^4F$	348 864	43.254
92	11/2	0.16 $4d^{10}(0S)4f^5(2H)^4H + 0.15 4d^{10}(0S)4f^5(3H)^2H + 0.12 4d^{10}(0S)4f^5(1I)^2I$	349 695	43.357
93	13/2	0.18 $4d^{10}(0S)4f^5(2I)^4I + 0.17 4d^{10}(0S)4f^5(3H)^4H + 0.13 4d^{10}(0S)4f^5(4K)^4K$	351 677	43.602
94	9/2	0.32 $4d^{10}(0S)4f^5(2H)^4H + 0.11 4d^{10}(0S)4f^5(2G)^2G + 0.06 4d^{10}(0S)4f^5(4G)^4G$	354 141	43.908
95	11/2	0.24 $4d^{10}(0S)4f^5(3H)^2H + 0.18 4d^{10}(0S)4f^5(3I)^2I + 0.08 4d^{10}(0S)4f^5(4G)^4G$	358 623	44.464
96	5/2	0.13 $4d^{10}(0S)4f^5(1F)^4F + 0.13 4d^{10}(0S)4f^5(3D)^2D + 0.10 4d^{10}(0S)4f^5(4F)^4F$	359 230	44.539
97	17/2	0.72 $4d^{10}(0S)4f^5(2L)^2L + 0.19 4d^{10}(0S)4f^5(3L)^2L + 0.02 4d^{10}(0S)4f^5(1L)^4L$	360 334	44.676
98	1/2	0.32 $4d^{10}(0S)4f^5(1D)^4D + 0.20 4d^{10}(0S)4f^5(4D)^4D + 0.15 4d^{10}(0S)4f^5(4P)^4P$	363 353	45.050
99	5/2	0.15 $4d^{10}(0S)4f^5(3F)^2F + 0.12 4d^{10}(0S)4f^5(4D)^2D + 0.12 4d^{10}(0S)4f^5(3D)^4D$	365 337	45.296
100	9/2	0.27 $4d^{10}(0S)4f^5(1I)^4I + 0.11 4d^{10}(0S)4f^5(4F)^4F + 0.09 4d^{10}(0S)4f^5(4G)^4G$	365 412	45.305

TABLE I: Continued.

No.	J	LS-composition	E (cm ⁻¹)	E (eV)
101	15/2	$0.21\ 4d^{10}(0S)\ 4f^5(4I)\ ^4I + 0.15\ 4d^{10}(0S)\ 4f^5(6H)\ ^6H + 0.13\ 4d^{10}(0S)\ 4f^5(4K)\ ^4K$	366 432	45.432
102	13/2	$0.20\ 4d^{10}(0S)\ 4f^5(2I)\ ^2I + 0.12\ 4d^{10}(0S)\ 4f^5(4I)\ ^2I + 0.10\ 4d^{10}(0S)\ 4f^5(2I)\ ^2I$	367 945	45.619
103	7/2	$0.17\ 4d^{10}(0S)\ 4f^5(1F)\ ^4F + 0.16\ 4d^{10}(0S)\ 4f^5(7F)\ ^2F + 0.11\ 4d^{10}(0S)\ 4f^5(3D)\ ^4D$	370 765	45.969
104	3/2	$0.18\ 4d^{10}(0S)\ 4f^5(2P)\ ^2P + 0.13\ 4d^{10}(0S)\ 4f^5(4F)\ ^4F + 0.12\ 4d^{10}(0S)\ 4f^5(3D)\ ^4D$	371 118	46.013
105	11/2	$0.31\ 4d^{10}(0S)\ 4f^5(2I)\ ^2I + 0.12\ 4d^{10}(0S)\ 4f^5(4H)\ ^4H + 0.11\ 4d^{10}(0S)\ 4f^5(4G)\ ^4G$	371 873	46.106
106	5/2	$0.20\ 4d^{10}(0S)\ 4f^5(4P)\ ^4P + 0.11\ 4d^{10}(0S)\ 4f^5(4D)\ ^4D + 0.09\ 4d^{10}(0S)\ 4f^5(2D)\ ^2D$	375 770	46.590
107	9/2	$0.33\ 4d^{10}(0S)\ 4f^5(2H)\ ^2H + 0.14\ 4d^{10}(0S)\ 4f^5(4H)\ ^4H + 0.09\ 4d^{10}(0S)\ 4f^5(4H)\ ^4H$	376 724	46.708
108	13/2	$0.23\ 4d^{10}(0S)\ 4f^5(3I)\ ^4I + 0.16\ 4d^{10}(0S)\ 4f^5(2K)\ ^2K + 0.12\ 4d^{10}(0S)\ 4f^5(4K)\ ^2K$	376 931	46.733
109	7/2	$0.17\ 4d^{10}(0S)\ 4f^5(4G)\ ^2G + 0.12\ 4d^{10}(0S)\ 4f^5(2H)\ ^4H + 0.08\ 4d^{10}(0S)\ 4f^5(3D)\ ^4D$	384 710	47.698
110	7/2	$0.13\ 4d^{10}(0S)\ 4f^5(4F)\ ^4F + 0.09\ 4d^{10}(0S)\ 4f^5(2F)\ ^4F + 0.09\ 4d^{10}(0S)\ 4f^5(3H)\ ^4H$	386 749	47.951
111	9/2	$0.17\ 4d^{10}(0S)\ 4f^5(2H)\ ^2H + 0.12\ 4d^{10}(0S)\ 4f^5(4G)\ ^2G + 0.09\ 4d^{10}(0S)\ 4f^5(4G)\ ^4G$	387 146	48.000
112	15/2	$0.24\ 4d^{10}(0S)\ 4f^5(2K)\ ^2K + 0.14\ 4d^{10}(0S)\ 4f^5(3K)\ ^2K + 0.12\ 4d^{10}(0S)\ 4f^5(4K)\ ^2K$	387 150	48.000
113	11/2	$0.18\ 4d^{10}(0S)\ 4f^5(2G)\ ^4G + 0.11\ 4d^{10}(0S)\ 4f^5(3I)\ ^2I + 0.10\ 4d^{10}(0S)\ 4f^5(2I)\ ^2I$	388 268	48.139
114	17/2	$0.28\ 4d^{10}(0S)\ 4f^5(1K)\ ^4K + 0.25\ 4d^{10}(0S)\ 4f^5(2M)\ ^2M + 0.13\ 4d^{10}(0S)\ 4f^5(1L)\ ^2L$	388 995	48.229
115	1/2	$0.36\ 4d^{10}(0S)\ 4f^5(1P)\ ^4P + 0.19\ 4d^{10}(0S)\ 4f^5(2P)\ ^2P + 0.14\ 4d^{10}(0S)\ 4f^5(2D)\ ^4D$	389 298	48.267
116	13/2	$0.28\ 4d^{10}(0S)\ 4f^5(2H)\ ^4H + 0.13\ 4d^{10}(0S)\ 4f^5(4K)\ ^4K + 0.11\ 4d^{10}(0S)\ 4f^5(3I)\ ^2I$	394 668	48.933
117	3/2	$0.16\ 4d^{10}(0S)\ 4f^5(4F)\ ^4F + 0.13\ 4d^{10}(0S)\ 4f^5(5D)\ ^2D + 0.10\ 4d^{10}(0S)\ 4f^5(2D)\ ^2D$	399 680	49.554
118	9/2	$0.14\ 4d^{10}(0S)\ 4f^5(6G)\ ^2G + 0.12\ 4d^{10}(0S)\ 4f^5(3H)\ ^4H + 0.10\ 4d^{10}(0S)\ 4f^5(2G)\ ^2G$	400 497	49.655
119	7/2	$0.11\ 4d^{10}(0S)\ 4f^5(1H)\ ^4H + 0.10\ 4d^{10}(0S)\ 4f^5(4F)\ ^4F + 0.07\ 4d^{10}(0S)\ 4f^5(3F)\ ^2F$	400 987	49.716
120	7/2	$0.12\ 4d^{10}(0S)\ 4f^5(2H)\ ^4H + 0.09\ 4d^{10}(0S)\ 4f^5(4G)\ ^4G + 0.08\ 4d^{10}(0S)\ 4f^5(3G)\ ^4G$	403 280	50.000
121	17/2	$0.48\ 4d^{10}(0S)\ 4f^5(2K)\ ^4K + 0.26\ 4d^{10}(0S)\ 4f^5(2M)\ ^2M + 0.09\ 4d^{10}(0S)\ 4f^5(4L)\ ^4L$	403 661	50.048
122	19/2	$0.32\ 4d^{10}(0S)\ 4f^5(1M)\ ^2M + 0.30\ 4d^{10}(0S)\ 4f^5(4L)\ ^4L + 0.18\ 4d^{10}(0S)\ 4f^5(2M)\ ^2M$	406 027	50.341
123	5/2	$0.16\ 4d^{10}(0S)\ 4f^5(2P)\ ^4P + 0.12\ 4d^{10}(0S)\ 4f^5(4F)\ ^4F + 0.11\ 4d^{10}(0S)\ 4f^5(4F)\ ^4F$	406 121	50.353
124	21/2	$0.54\ 4d^{10}(0S)\ 4f^5(2N)\ ^2N + 0.24\ 4d^{10}(0S)\ 4f^5(2O)\ ^2O + 0.21\ 4d^{10}(0S)\ 4f^5(4M)\ ^4M$	408 548	50.654
125	13/2	$0.29\ 4d^{10}(0S)\ 4f^5(2K)\ ^2K + 0.24\ 4d^{10}(0S)\ 4f^5(2I)\ ^2I + 0.17\ 4d^{10}(0S)\ 4f^5(3J)\ ^2I$	411 044	50.963
126	9/2	$0.13\ 4d^{10}(0S)\ 4f^5(6G)\ ^2G + 0.13\ 4d^{10}(0S)\ 4f^5(3G)\ ^4G + 0.09\ 4d^{10}(0S)\ 4f^5(4G)\ ^4G$	411 064	50.966
127	19/2	$0.61\ 4d^{10}(0S)\ 4f^5(2M)\ ^2M + 0.36\ 4d^{10}(0S)\ 4f^5(1M)\ ^2M$	412 462	51.139
128	11/2	$0.23\ 4d^{10}(0S)\ 4f^5(1H)\ ^4H + 0.12\ 4d^{10}(0S)\ 4f^5(3H)\ ^2H + 0.07\ 4d^{10}(0S)\ 4f^5(4H)\ ^2H$	413 336	51.247
129	1/2	$0.30\ 4d^{10}(0S)\ 4f^5(2P)\ ^2P + 0.18\ 4d^{10}(0S)\ 4f^5(3D)\ ^4D + 0.15\ 4d^{10}(0S)\ 4f^5(2P)\ ^2P$	414 336	51.371
130	5/2	$0.17\ 4d^{10}(0S)\ 4f^5(4D)\ ^4D + 0.16\ 4d^{10}(0S)\ 4f^5(2F)\ ^2F + 0.14\ 4d^{10}(0S)\ 4f^5(2D)\ ^2D$	418 426	51.878
131	15/2	$0.34\ 4d^{10}(0S)\ 4f^5(3K)\ ^2K + 0.14\ 4d^{10}(0S)\ 4f^5(4K)\ ^2K + 0.14\ 4d^{10}(0S)\ 4f^5(2K)\ ^4K$	418 804	51.925
132	11/2	$0.22\ 4d^{10}(0S)\ 4f^5(5H)\ ^2H + 0.15\ 4d^{10}(0S)\ 4f^5(2I)\ ^2I + 0.11\ 4d^{10}(0S)\ 4f^5(4H)\ ^4H$	420 383	52.121
133	3/2	$0.29\ 4d^{10}(0S)\ 4f^5(4D)\ ^4D + 0.29\ 4d^{10}(0S)\ 4f^5(1F)\ ^4F + 0.15\ 4d^{10}(0S)\ 4f^5(4D)\ ^4D$	421 095	52.209
134	9/2	$0.28\ 4d^{10}(0S)\ 4f^5(4F)\ ^4F + 0.18\ 4d^{10}(0S)\ 4f^5(2H)\ ^4H + 0.10\ 4d^{10}(0S)\ 4f^5(4F)\ ^4F$	423 220	52.473
135	5/2	$0.13\ 4d^{10}(0S)\ 4f^5(1F)\ ^2F + 0.13\ 4d^{10}(0S)\ 4f^5(7F)\ ^2F + 0.12\ 4d^{10}(0S)\ 4f^5(4F)\ ^4F$	426 066	52.826
136	13/2	$0.19\ 4d^{10}(0S)\ 4f^5(3I)\ ^2I + 0.14\ 4d^{10}(0S)\ 4f^5(2I)\ ^2I + 0.11\ 4d^{10}(0S)\ 4f^5(1I)\ ^2I$	431 042	53.442
137	9/2	$0.18\ 4d^{10}(0S)\ 4f^5(4H)\ ^2H + 0.17\ 4d^{10}(0S)\ 4f^5(4F)\ ^4F + 0.10\ 4d^{10}(0S)\ 4f^5(7H)\ ^2H$	431 992	53.560

TABLE I: Continued.

No.	J	LS-composition	E (cm ⁻¹)	E (eV)
138	11/2	0.25 $4d^{10}(0S)4f^5(2I)^2I + 0.20 4d^{10}(0S)4f^5(4H)^4H + 0.18 4d^{10}(0S)4f^5(4G)^4G$	433 367	53.731
139	15/2	0.30 $4d^{10}(0S)4f^5(2K)^2K + 0.17 4d^{10}(0S)4f^5(2L)^2L + 0.14 4d^{10}(0S)4f^5(2L)^2L$	433 924	53.800
140	3/2	0.19 $4d^{10}(0S)4f^5(4P)^4P + 0.18 4d^{10}(0S)4f^5(4F)^4F + 0.09 4d^{10}(0S)4f^5(4P)^2P$	435 170	53.954
141	7/2	0.22 $4d^{10}(0S)4f^5(3G)^2G + 0.20 4d^{10}(0S)4f^5(5F)^2F + 0.10 4d^{10}(0S)4f^5(2F)^2F$	436 081	54.067
142	1/2	0.28 $4d^{10}(0S)4f^5(2P)^2P + 0.26 4d^{10}(0S)4f^5(3D)^4D + 0.25 4d^{10}(0S)4f^5(4D)^4D$	441 616	54.753
143	7/2	0.30 $4d^{10}(0S)4f^5(4F)^2F + 0.11 4d^{10}(0S)4f^5(5F)^2F + 0.11 4d^{10}(0S)4f^5(4D)^4D$	445 673	55.256
144	3/2	0.21 $4d^{10}(0S)4f^5(4P)^4P + 0.15 4d^{10}(0S)4f^5(4S)^4S + 0.13 4d^{10}(0S)4f^5(4F)^4F$	447 007	55.422
145	9/2	0.17 $4d^{10}(0S)4f^5(3G)^2G + 0.16 4d^{10}(0S)4f^5(4H)^2H + 0.11 4d^{10}(0S)4f^5(4F)^4F$	447 321	55.461
146	13/2	0.23 $4d^{10}(0S)4f^5(4I)^2I + 0.17 4d^{10}(0S)4f^5(2I)^2I + 0.14 4d^{10}(0S)4f^5(5K)^2K$	448 301	55.582
147	15/2	0.24 $4d^{10}(0S)4f^5(3L)^2L + 0.21 4d^{10}(0S)4f^5(4I)^4I + 0.20 4d^{10}(0S)4f^5(4I)^4I$	449 525	55.734
148	11/2	0.29 $4d^{10}(0S)4f^5(4I)^4I + 0.16 4d^{10}(0S)4f^5(6H)^2H + 0.13 4d^{10}(0S)4f^5(4G)^4G$	451 255	55.949
149	5/2	0.32 $4d^{10}(0S)4f^5(3F)^2F + 0.17 4d^{10}(0S)4f^5(7F)^2F + 0.14 4d^{10}(0S)4f^5(3D)^2D$	451 765	56.012
150	9/2	0.14 $4d^{10}(0S)4f^5(3F)^4F + 0.11 4d^{10}(0S)4f^5(3H)^2H + 0.10 4d^{10}(0S)4f^5(3G)^2G$	454 196	56.313
151	5/2	0.19 $4d^{10}(0S)4f^5(4D)^4D + 0.18 4d^{10}(0S)4f^5(4G)^4G + 0.14 4d^{10}(0S)4f^5(4P)^4P$	456 724	56.627
152	3/2	0.20 $4d^{10}(0S)4f^5(3P)^2P + 0.12 4d^{10}(0S)4f^5(4S)^4S + 0.11 4d^{10}(0S)4f^5(2D)^2D$	457 495	56.722
153	7/2	0.17 $4d^{10}(0S)4f^5(5G)^2G + 0.13 4d^{10}(0S)4f^5(4G)^2G + 0.11 4d^{10}(0S)4f^5(6G)^2G$	457 513	56.724
154	13/2	0.38 $4d^{10}(0S)4f^5(5I)^2I + 0.10 4d^{10}(0S)4f^5(3H)^4H + 0.09 4d^{10}(0S)4f^5(2K)^4K$	461 925	57.271
155	11/2	0.27 $4d^{10}(0S)4f^5(2I)^2I + 0.14 4d^{10}(0S)4f^5(4G)^4G + 0.14 4d^{10}(0S)4f^5(4G)^4G$	468 166	58.045
156	5/2	0.21 $4d^{10}(0S)4f^5(1F)^4F + 0.18 4d^{10}(0S)4f^5(3F)^2F + 0.10 4d^{10}(0S)4f^5(2F)^2F$	470 554	58.341
157	9/2	0.18 $4d^{10}(0S)4f^5(2H)^2H + 0.15 4d^{10}(0S)4f^5(3H)^2H + 0.12 4d^{10}(0S)4f^5(6H)^2H$	471 029	58.400
158	7/2	0.24 $4d^{10}(0S)4f^5(4G)^2G + 0.14 4d^{10}(0S)4f^5(6G)^2G + 0.10 4d^{10}(0S)4f^5(4F)^2F$	474 761	58.863
159	3/2	0.25 $4d^{10}(0S)4f^5(4D)^2D + 0.14 4d^{10}(0S)4f^5(2P)^2P + 0.11 4d^{10}(0S)4f^5(4S)^4S$	475 131	58.909
160	11/2	0.23 $4d^{10}(0S)4f^5(5H)^2H + 0.12 4d^{10}(0S)4f^5(6H)^2H + 0.10 4d^{10}(0S)4f^5(5I)^2I$	480 938	59.629
161	15/2	0.25 $4d^{10}(0S)4f^5(2L)^2L + 0.14 4d^{10}(0S)4f^5(4K)^2K + 0.14 4d^{10}(0S)4f^5(1I)^4I$	494 281	61.283
162	5/2	0.19 $4d^{10}(0S)4f^5(3F)^2F + 0.12 4d^{10}(0S)4f^5(4G)^4G + 0.11 4d^{10}(0S)4f^5(4D)^4D$	495 243	61.402
163	13/2	0.35 $4d^{10}(0S)4f^5(4I)^4I + 0.12 4d^{10}(0S)4f^5(5I)^2I + 0.08 4d^{10}(0S)4f^5(1K)^2K$	498 809	61.844
164	7/2	0.18 $4d^{10}(0S)4f^5(1G)^4G + 0.15 4d^{10}(0S)4f^5(1F)^4F + 0.13 4d^{10}(0S)4f^5(6G)^2G$	500 479	62.052
165	11/2	0.37 $4d^{10}(0S)4f^5(1H)^2H + 0.14 4d^{10}(0S)4f^5(2I)^2I + 0.10 4d^{10}(0S)4f^5(7H)^2H$	502 118	62.255
166	7/2	0.27 $4d^{10}(0S)4f^5(4D)^4D + 0.26 4d^{10}(0S)4f^5(2G)^2G + 0.07 4d^{10}(0S)4f^5(2H)^4H$	505 232	62.641
167	5/2	0.25 $4d^{10}(0S)4f^5(6F)^2F + 0.15 4d^{10}(0S)4f^5(4G)^4G + 0.12 4d^{10}(0S)4f^5(2D)^2D$	505 252	62.643
168	3/2	0.18 $4d^{10}(0S)4f^5(1D)^4D + 0.18 4d^{10}(0S)4f^5(2P)^2P + 0.12 4d^{10}(0S)4f^5(3P)^2P$	513 160	63.624
169	1/2	0.34 $4d^{10}(0S)4f^5(4P)^2P + 0.23 4d^{10}(0S)4f^5(3P)^2P + 0.17 4d^{10}(0S)4f^5(1P)^2P$	514 872	63.836
170	9/2	0.19 $4d^{10}(0S)4f^5(4F)^4F + 0.15 4d^{10}(0S)4f^5(5G)^2G + 0.15 4d^{10}(0S)4f^5(2H)^2H$	515 040	63.857
171	15/2	0.48 $4d^{10}(0S)4f^5(1K)^2K + 0.17 4d^{10}(0S)4f^5(4I)^4I + 0.14 4d^{10}(0S)4f^5(4K)^2K$	519 238	64.377
172	17/2	0.58 $4d^{10}(0S)4f^5(2L)^2L + 0.21 4d^{10}(0S)4f^5(2M)^2M + 0.10 4d^{10}(0S)4f^5(4K)^4K$	522 902	64.832
173	9/2	0.17 $4d^{10}(0S)4f^5(2G)^2G + 0.10 4d^{10}(0S)4f^5(4F)^4F + 0.09 4d^{10}(0S)4f^5(2G)^2G$	525 777	65.188
174	13/2	0.44 $4d^{10}(0S)4f^5(1I)^2I + 0.16 4d^{10}(0S)4f^5(2K)^2K + 0.12 4d^{10}(0S)4f^5(4H)^4H$	529 134	65.604

TABLE I: Continued.

No.	J	LS-composition	E (cm $^{-1}$)	E (eV)
175	9/2	$0.21\ 4d^{10}(^1_0S)\ 4f^5(^2_7H)\ ^2H + 0.17\ 4d^{10}(^1_0S)\ 4f^5(^2_1H)\ ^2H + 0.11\ 4d^{10}(^1_0S)\ 4f^5(^2_2G)\ ^2G$	531 591	65.909
176	7/2	$0.15\ 4d^{10}(^1_0S)\ 4f^5(^4_4G)\ ^4G + 0.13\ 4d^{10}(^1_0S)\ 4f^5(^4_1F)\ ^4F + 0.11\ 4d^{10}(^1_0S)\ 4f^5(^2_2F)\ ^2F$	532 063	65.967
177	11/2	$0.16\ 4d^{10}(^1_0S)\ 4f^5(^2_1I)\ ^2I + 0.13\ 4d^{10}(^1_0S)\ 4f^5(^4_4G)\ ^4G + 0.11\ 4d^{10}(^1_0S)\ 4f^5(^2_6H)\ ^2H$	535 205	66.357
178	3/2	$0.21\ 4d^{10}(^1_0S)\ 4f^5(^2_2P)\ ^2P + 0.20\ 4d^{10}(^1_0S)\ 4f^5(^2_4D)\ ^2D + 0.11\ 4d^{10}(^1_0S)\ 4f^5(^2_3D)\ ^2D$	536 820	66.557
179	9/2	$0.24\ 4d^{10}(^1_0S)\ 4f^5(^4_1G)\ ^4G + 0.12\ 4d^{10}(^1_0S)\ 4f^5(^2_1G)\ ^2G + 0.09\ 4d^{10}(^1_0S)\ 4f^5(^2_2H)\ ^2H$	543 184	67.346
180	15/2	$0.28\ 4d^{10}(^1_0S)\ 4f^5(^2_5K)\ ^2K + 0.18\ 4d^{10}(^1_0S)\ 4f^5(^2_1K)\ ^2K + 0.14\ 4d^{10}(^1_0S)\ 4f^5(^4_1I)\ ^4I$	543 477	67.383
181	5/2	$0.12\ 4d^{10}(^1_0S)\ 4f^5(^2_4D)\ ^2D + 0.12\ 4d^{10}(^1_0S)\ 4f^5(^2_7F)\ ^2F + 0.10\ 4d^{10}(^1_0S)\ 4f^5(^2_4F)\ ^2F$	555 103	68.824
182	3/2	$0.39\ 4d^{10}(^1_0S)\ 4f^5(^2_1D)\ ^2D + 0.12\ 4d^{10}(^1_0S)\ 4f^5(^4_1F)\ ^4F + 0.10\ 4d^{10}(^1_0S)\ 4f^5(^2_4P)\ ^2P$	558 270	69.217
183	11/2	$0.17\ 4d^{10}(^1_0S)\ 4f^5(^2_4I)\ ^2I + 0.17\ 4d^{10}(^1_0S)\ 4f^5(^2_7H)\ ^2H + 0.13\ 4d^{10}(^1_0S)\ 4f^5(^2_1H)\ ^2H$	560 638	69.510
184	7/2	$0.21\ 4d^{10}(^1_0S)\ 4f^5(^2_1G)\ ^2G + 0.16\ 4d^{10}(^1_0S)\ 4f^5(^2_6F)\ ^2F + 0.13\ 4d^{10}(^1_0S)\ 4f^5(^2_2G)\ ^2G$	574 583	71.239
185	5/2	$0.45\ 4d^{10}(^1_0S)\ 4f^5(^2_2F)\ ^2F + 0.17\ 4d^{10}(^1_0S)\ 4f^5(^2_6F)\ ^2F + 0.08\ 4d^{10}(^1_0S)\ 4f^5(^4_4F)\ ^4F$	575 751	71.384
186	13/2	$0.37\ 4d^{10}(^1_0S)\ 4f^5(^2_4K)\ ^2K + 0.26\ 4d^{10}(^1_0S)\ 4f^5(^2_1K)\ ^2K + 0.20\ 4d^{10}(^1_0S)\ 4f^5(^2_5I)\ ^2I$	576 453	71.471
187	9/2	$0.31\ 4d^{10}(^1_0S)\ 4f^5(^2_1G)\ ^2G + 0.22\ 4d^{10}(^1_0S)\ 4f^5(^2_4G)\ ^2G + 0.21\ 4d^{10}(^1_0S)\ 4f^5(^2_1H)\ ^2H$	579 634	71.866
188	3/2	$0.46\ 4d^{10}(^1_0S)\ 4f^5(^2_1P)\ ^2P + 0.15\ 4d^{10}(^1_0S)\ 4f^5(^2_2D)\ ^2D + 0.13\ 4d^{10}(^1_0S)\ 4f^5(^2_5D)\ ^2D$	588 320	72.942
189	7/2	$0.38\ 4d^{10}(^1_0S)\ 4f^5(^2_2F)\ ^2F + 0.19\ 4d^{10}(^1_0S)\ 4f^5(^2_6G)\ ^2G + 0.13\ 4d^{10}(^1_0S)\ 4f^5(^2_1F)\ ^2F$	590 723	73.240
190	5/2	$0.24\ 4d^{10}(^1_0S)\ 4f^5(^2_5D)\ ^2D + 0.17\ 4d^{10}(^1_0S)\ 4f^5(^2_7F)\ ^2F + 0.06\ 4d^{10}(^1_0S)\ 4f^5(^2_5F)\ ^2F$	604 231	74.915
191	1/2	$0.56\ 4d^{10}(^1_0S)\ 4f^5(^2_1P)\ ^2P + 0.23\ 4d^{10}(^1_0S)\ 4f^5(^2_3P)\ ^2P + 0.14\ 4d^{10}(^1_0S)\ 4f^5(^2_2P)\ ^2P$	616 076	76.384
192	7/2	$0.27\ 4d^{10}(^1_0S)\ 4f^5(^2_1G)\ ^2G + 0.17\ 4d^{10}(^1_0S)\ 4f^5(^2_6F)\ ^2F + 0.12\ 4d^{10}(^1_0S)\ 4f^5(^2_5F)\ ^2F$	623 479	77.302
193	9/2	$0.24\ 4d^{10}(^1_0S)\ 4f^5(^2_2H)\ ^2H + 0.20\ 4d^{10}(^1_0S)\ 4f^5(^2_6G)\ ^2G + 0.09\ 4d^{10}(^1_0S)\ 4f^5(^2_1G)\ ^2G$	626 993	77.737
194	11/2	$0.54\ 4d^{10}(^1_0S)\ 4f^5(^2_2H)\ ^2H + 0.25\ 4d^{10}(^1_0S)\ 4f^5(^2_7H)\ ^2H + 0.06\ 4d^{10}(^1_0S)\ 4f^5(^2_1H)\ ^2H$	628 421	77.914
195	3/2	$0.40\ 4d^{10}(^1_0S)\ 4f^5(^2_2D)\ ^2D + 0.18\ 4d^{10}(^1_0S)\ 4f^5(^2_5D)\ ^2D + 0.13\ 4d^{10}(^1_0S)\ 4f^5(^2_4P)\ ^2P$	672 448	83.373
196	5/2	$0.25\ 4d^{10}(^1_0S)\ 4f^5(^2_2D)\ ^2D + 0.23\ 4d^{10}(^1_0S)\ 4f^5(^2_1D)\ ^2D + 0.18\ 4d^{10}(^1_0S)\ 4f^5(^2_1F)\ ^2F$	676 505	83.876
197	7/2	$0.59\ 4d^{10}(^1_0S)\ 4f^5(^2_1F)\ ^2F + 0.21\ 4d^{10}(^1_0S)\ 4f^5(^2_6F)\ ^2F + 0.04\ 4d^{10}(^1_0S)\ 4f^5(^2_2F)\ ^2F$	715 351	88.692
198	5/2	$0.33\ 4d^{10}(^1_0S)\ 4f^5(^2_1F)\ ^2F + 0.27\ 4d^{10}(^1_0S)\ 4f^5(^2_2D)\ ^2D + 0.14\ 4d^{10}(^1_0S)\ 4f^5(^2_5D)\ ^2D$	721 528	89.458

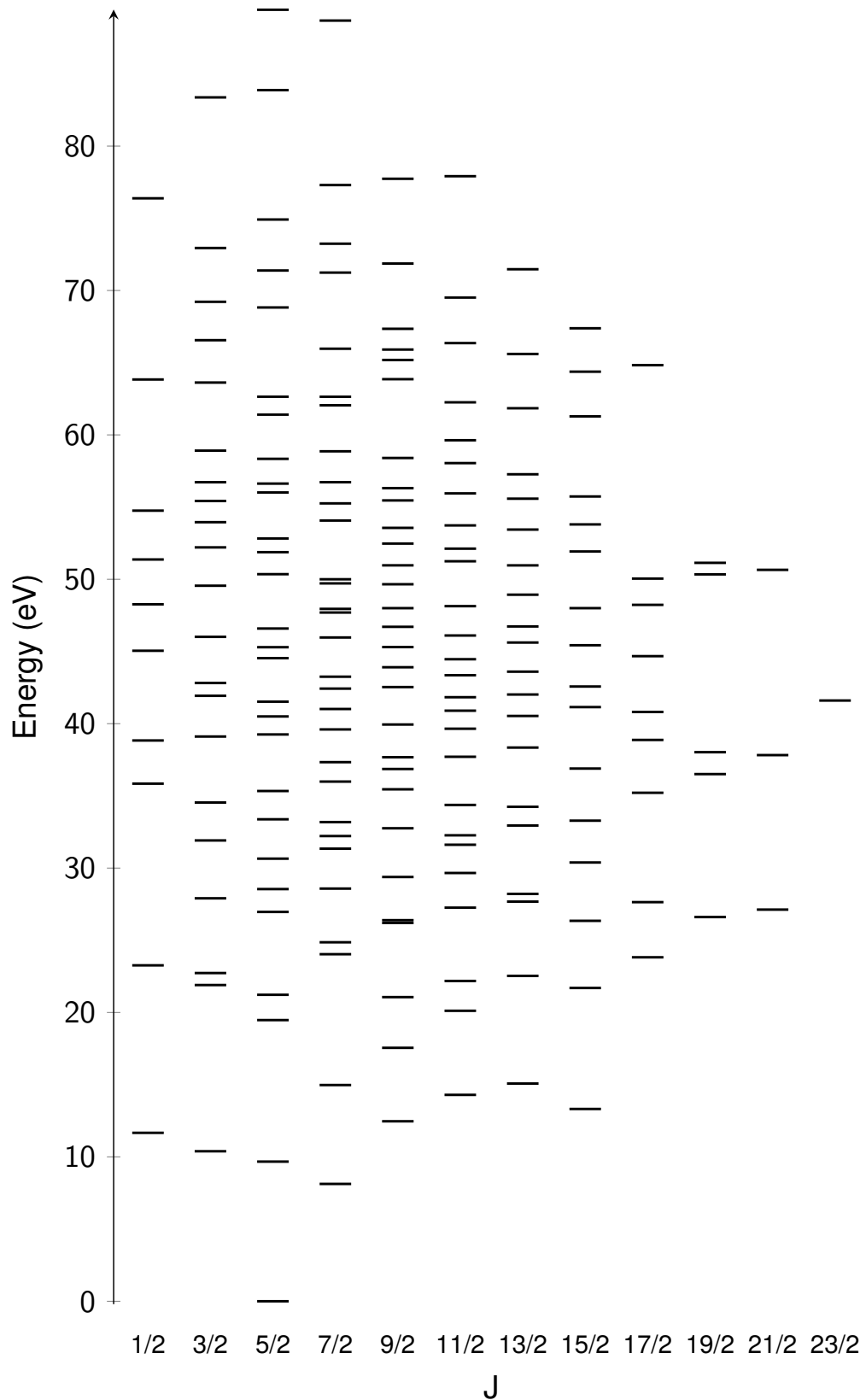


FIG. 1. Energy level diagram for all states of the $[Kr]4d^{10}4f^5$ configuration in Th^{39+} .

COLLISIONAL-RADIATIVE MODEL SIMULATIONS

In our Collisional-Radiative Model (CRM) simulations, conducted using the FAC code [1], we employed the so-called 'one-ion model' [2]. In this model, only radiative transition rates and cross sections for collisional excitations are considered in calculating the level populations for a given ion. The electron configurations considered in the CRM simulations are listed in Table II. The model includes radiative transitions of types E1, E2, M1, and M2 between levels of the 'gr' group, as well as radiative transitions of type E1 between levels of the 'exc' and 'gr' groups. Collisional excitations between levels within the 'gr' group and between levels of the 'gr' and 'exc' groups are also included. Since the ionization energy for the Th^{38+} ion is 1680 eV [3], we assumed an electron temperature of $T_e = 2 \text{ keV}$ in the CRM simulations. The assumed electron density of $d_e = 10^{12} \text{ cm}^{-3}$ is a typical value for EBIT devices.

TABLE II. Configurations included in the CRM simulations.

Group	Electron configurations ([Kr] core)	Number of levels
gr	$4d^{10} 4f^5$	198
exc	$4d^9 4f^6$, $4d^{10} 4f^4 5(s,p,d,f)^1$, $4d^{10} 4f^3 5(s,p)^1 5(s,p)^1$, $4d^9 4f^5 5(s,p)^1$	21557

* Karol.Koziol@ncbj.gov.pl

† Jacek.Rzadkiewicz@ncbj.gov.pl

- [1] M. F. Gu, [Canadian Journal of Physics 86, 675 \(2008\)](#).
- [2] M. F. Gu, [The Astrophysical Journal 582, 1241 \(2003\)](#).
- [3] A. E. Kramida, Y.Ralchenko, J. Reader, and N. A. Team, [NIST Atomic Spectra Database](#) (2024).